J Med Syst (2016) 40: 279
DOI 10.1007/s10916-016-0635-x

Superharmonic Imaging for Medical Ultrasound: a Review

Narendra D. Londhe[1] · **Jasjit S. Suri**[2,3]

Received: 26 June 2016 / Accepted: 12 October 2016 / Published online: 27 October 2016

Abstract Ultrasound with harmonics has emerged as an exceptional alternative to competitively low resolution fundamental ultrasound imaging. The use of second harmonic is already a trend now but higher harmonics are also being seen as even better option due to its improved resolution. The resolution improved with frequency but achieves penetration of reduced energy. The cumulative addition of higher harmonics during propagation yields higher harmonics giving better resolution with adequate penetration. This paper summarizes the progress of such similar decade old harmonic ultrasound imaging technique i.e., superharmonic imaging (SHI) geared towards medical field. It comprises of harmonics higher than second harmonic preferably up to 5th harmonic. We conclude that SHI can be an advanced ultrasound imaging with comprehensive high resolution and adequate penetration depth on sole and coded modes.

Keyword Ultrasonic imaging · Superharmonics · Transducer · Nonlinear propagation · Coded excitation

This article is part of the Topical Collection on *Transactional Processing Systems*

✉ Jasjit S. Suri
Jasjit.Suri@atheropoint.com

[1] Department of Electrical Engineering, NIT Raipur, Raipur, Chhattisgarh, India

[2] Point-of-Care Devices, Global Biomedical Technologies, Inc., Roseville, CA, USA

[3] Monitoring and Diagnostic Division, AtheroPoint™, Roseville, CA, USA

Introduction

In the past years there has been striking technological developments and growth in ultrasound imaging. This has resulted in triumphant 3-D ultrasound imaging, tissue harmonic imaging (THI), contrast-based harmonic imaging, and superharmonic imaging (SHI). Tissue harmonic imaging is an established imaging modality in the present era due to its improved image quality in addition to its real time imaging, ergonomic, affordable cost and harmless nature. Ultrasound imaging facilitates physicians to respond critical clinical questions in emergency at the bedside which would decipher into improved diagnosis and treatment. In spite of its advantages, it still faces great challenges in terms of resolution from very high resolution imaging devices like CT, MRI.

At present, two modes of harmonic imaging are present: (i) contrast-based and (ii) tissue-based. In contrast-based harmonic imaging, the harmonics are generated out of oscillating contrast agents while in tissue-based harmonic imaging (THI), the harmonics originate from nonlinear propagation of ultrasound through a biological medium [1]. In both modes, the second harmonic frequency is adapted for the image formation. The harmonic signals used in contrast-based harmonic imaging do not come from the ultrasound system itself. These harmonics are produced as a result of interactions of ultrasound waves with tissues or contrast agents. In case of contrast harmonic imaging, the patient is injected with contrast agents (microbubbles) which then interacts with ultrasonic pulses gives two kinds of responses. Firstly, reflections of ultrasound pulses due to acoustic impedance difference between bubbles and the surrounding tissues. Secondly, the response due to vibrations of bubbles in response of shock from the ultrasonic pulses. These vibrations have frequency twice the frequency of original ultrasound pulses. This confines the bandwidth available for imaging so that the received harmonic signal can be separated from the fundamental. The

overlapping of the fundamental with second harmonic restricts the complete separation of harmonic from the received response. Thus, in contrast based harmonic imaging a narrower bandwidth is used.

Tissue harmonic imaging starts with an exposure of tissue medium with ultrasound of a specific transmitted frequency. Harmonic waves start to generate within the tissue and keep growing further to a position of maximal intensity before they get reduced due to attenuation [2–5]. Harmonic imaging gives potential advantages that it includes improved axial resolution due to shorter wavelength, better lateral resolution due to improved focusing with higher frequencies, and fewer artifacts compared to conventional [6, 7].

Indeed harmonic imaging also suffers from few limitations like: low signal-to-noise ratio, the presence of side-lobe levels and the harmonic leakage [8]. The second harmonic echoes used to be of low amplitude which makes imaging difficult as it needs the transducer of high sensitivity and wide frequency range. But this leads to increased side-lobe levels and harmonic leakage with an increase in beam width profile. On the contrary, the transmitting narrower beam reduces the axial resolution because of the overlap of fundamental and second harmonic beam profiles.

Though the use of harmonics enhances resolution, harmonic imaging merely uses second harmonic for imaging out of numerous higher order harmonics generated due to nonlinear propagation. However it is possible to take advantage of higher order harmonics and further increase the image quality. A decade ago, a new imaging technique known as superharmonic imaging (SHI) [9] was proposed. This has shown possibilities of better ultrasound imaging. As it uses the linear sum of higher harmonics, the improvement in resolution with better signal-to-noise ratio and adequate penetration depth is observed. So, for SHI, the transmission of narrow beam of lower frequency is transmitted and echoes received are of higher frequencies. Thus, in SHI, the wideband filter used is primarily whose field gives a linear sum which ultimately generates high resolution superharmonic images [10, 11].

The research experiments [10–14] confirmed that SHI deserves next to be ultrasound imaging modality after fundamental and second harmonic based ultrasound imaging. Though it is still not in clinical studies, but exhaustive research is going on with promising future.

The SHI is in existence for almost 12 years now. A typical cycle for a product to commercialize is 5–10 years and the world to start using it is 10–15 years and even 20 years sometime. This technology is new and has vast scope of improvement; therefore the possibility of clinical application is slow. However SHI due to contrast agent and tissue nonlinearity both have been studied and its applications in echocardiography [8], abdominal sonography [12], and intravascular ultrasound imaging [15] have been reported. Attempts have been made for successful design of the SHI probe for the above applications [16, 17].

Next to that it has also been investigated with coded excitation [18–20] which has given further advancement to it. The generalized block diagram for superharmonic imaging with or without coded excitations is depicted below in Fig. 1. It has been shown here the specialized instrumentation, beam formation and further enhancement using coded excitation.

This paper presents deep insight of the works done in the establishment of superharmonic imaging. Its journey started in 2002 by proposing it first time by Bouakaz et al. [9] with contrast agent for higher harmonics generation and continued with nonlinear behavior of tissue medium for higher harmonics generation in 2003 [10]. We will present the glimpses of such works on superharmonic imaging in the last decade. Majorly, we will be addressing evolution, customized instrumentation, numerical models, in-vitro and in-vivo studies, beam optimization and clinical aspects of superharmonic imaging.

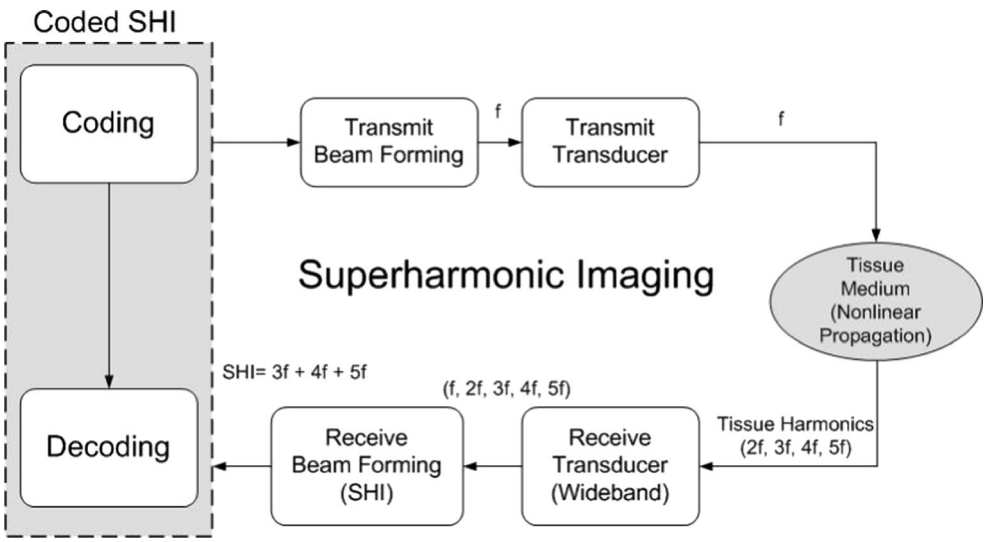

Fig. 1 Generalized super harmonic imaging

Establishment

Even though, the conventional ultrasound imaging is harmless and economic when using harmonic variant based on the second harmonic, but this is not truly generalized for all depths and frequencies. Thus clearly there is need for an improvement in quality. It is still convenient and second most widely used imaging modality in the world after X-rays. Its tortoise speed in the race of credibly developing imaging modalities like CT, MRI etc. is still going on, since 1942. During this period, its use of the fundamental frequency from the received response for imaging is changed to second harmonic and now to higher harmonics. The present era is already exposed to superharmonic imaging based on higher harmonics.

Bouakaz et al. [9] first presented the SHI as a combination of higher harmonics specifically third, fourth and fifth, that comes out of the nonlinear response of contrast bubbles. The SHI has been feasible due to their proposed phased array transducer which operates over a wide band to receive harmonics efficiently. The simulation for both nonlinear harmonics and contrast harmonics presented using KZK equation and Rayleigh-Plesset differential equation respectively. This has shown that the nonlinear higher harmonics are more dominant if the transmit frequency is high. While contrast due to higher harmonics at low transmit frequency is high, this results in a higher contrast to tissue ratio (CTR).

The dual frequency array transducer used here contains two different types of elements arranged in an interleaved pattern (odd and even elements). Out of 96 elements in the array, half odd elements work at around 2.8 MHz center frequency and 80 % bandwidth while half even elements have a center frequency of 0.9 MHz with a bandwidth of 50 %. The width of each of the element considered is 0.2 mm. As elements operate separately, separate transmission and reception modes are feasible. The lower frequency in transmission guarantees reduced tissue and contrast attenuation [6].

Moreover, in vitro measurements using ultrasound, contrast agents were carried out using the dual frequency probe operating in the superharmonic imaging mode. A tissue-mimicking flow phantom was used. The in vitro measurements (animal experiments) were performed and compared to contrast second harmonic to establish the optimal settings and parameters for improved contrast detection in the superharmonic mode. To extend this to a clinical spectrum, they also investigated cardiac echocardiography for 10 patients aged from 35 to 65 years [11]. They have found that along with high CTR, the clutters and noises are reduced in SHI and it gets adequate penetration depth and resolution.

In the next of Bouakaz et al. [10] the authors continued confirming the generation of superharmonic using nonlinear tissue harmonics. Water was often considered as the closest approximate of the soft tissues. They experimented on the phantom having the water cavity using the similar interleaved phased array transducer and compared with nonlinear KZK propagation model. The issue of low sensitivity and signal to noise ratio (SNR) in nonlinear tissue harmonics compared to contrast harmonics leads to confirm that the use of signal harmonics like in THI sacrifices the dynamic range and SNR. While inclusion of other higher harmonics together i.e., superharmonic has found receiving increased energy while taking advantage from the beam characteristics of these higher harmonics. Therefore, the combination of the higher harmonic components into a single superharmonic component instead of using a single harmonic frequency is a beneficial way of increasing the amount of detected energy compared to the second harmonic energy alone, while additionally preserving the advantages of the higher harmonics. The superharmonic energy level is often higher than the second harmonic energy level at important imaging distances, and in some situations it can be even higher than the energy level at the fundamental frequency, if different combinations of the superharmonic component are considered.

Array transducer for superharmonic imaging

The performance of current array transducers is satisfactory for second harmonic imaging. They have the significantly limited frequency bandwidth of 70 to 80 % of the center frequency, not suitable to perform imaging for harmonics higher than second. Superharmonics generate out due to cumulative addition of the higher harmonics specifically third, fourth and fifth. To image on receiving these higher frequency harmonics, a very wide band multi-frequency and higher sensitivity transducer is essential for receiving harmonics. These harmonics generate out of nonlinear propagation and available for imaging, are absent during transmission. So, Bouakaz et al. [16] proposed new interleaved and dual frequency phased array transducer topology along with SHI to assert its practical feasibility. Table 1 shows the literature survey of multi-frequency transducer that could be used for SHI.

First two novel ultrasound multi-frequency harmonic transducer arrays (MFHA's) for contrast enhanced second harmonic (THI) and sub-harmonic (SbHI) imaging have been designed by Forsberg et al. [26, 27] Both consist of 3 multi-element piezo-composite sub-arrays (X, Y & Z) accumulated in a curve giving mechanical focus of 5 cm. The center frequency for the sub-arrays is designed in such a way that fZ is twice of the fY which itself is twice of fX i.e. for example 2.5/5.0/10.0 MHz and 1.75/3.5/7.0 MHz. For SbHI, if Y sub-array transmitting then X is receiving and similarly from Z to Y. While for THI, if X sub-array transmitting then Y is receiving and similarly from Y to Z.

Specifically for SHI, a multi-frequency transducer was proposed in a new array design [16] along with superharmonic

Table 1 Literature survey on dual frequency array transducer topologies

Transducer topology	Design	Material	Advantage	Disadvantage
High bandwidth transducer [21]	Two active layers with different resonance frequencies on top of each other for each array element	Usually PZT or a PZT composite	1. limited total footprint of the array 2. ease of manufacture	Troughs in the frequency response of the transducer
Ultra broadband transducer [22]	One layer for transmission and other for reception	PZT layer for transmission and a PVDF layer for reception	guaranteed electromechanical decoupling	Poor sensitivity of PVDF
Horizontal stack topology [23]	Two low-frequency arrays are positioned laterally on both sides of a central high-frequency array	Usually PZT or a PZT composite	initial performance of each sub-array is not modified	1. Limited overlap of both acoustic beams 2. Increased footprint in the elevation dimension relative to a regular array design
Interleaved transducer array [16]	Even elements are used in transmission and the odd elements are used in reception	Usually PZT or a PZT composite	full overlap of the transmission and receive beams and a small footprint	1. relatively complicated to manufacture 2. its intrinsically reduced sensitivity,
Capacitive micro-machined ultrasound transducer (cMUT) [24]	A cavity is formed in a silicon substrate, and a thin layer suspended on the top of the cavity serves as a membrane on which a metallized layer acts an electrode to form necessary capacitance.	Silicon substrate	−6-dB bandwidths of 130 %	1. Difficult to attend high output pressures 2. their inherent nonlinearity, 3. relatively high crosstalk
Interleaved transducer array [25]	Interleaved dual frequency array	PZT (CTS 3203HD) for interleaved layers	efficient both in transmission and reception with well behaved transfer functions and a combined −6-dB bandwidth of 144 %	1. less cross talk 2. less variation in response 3. higher fundamental transmission efficiency, 4. improved sensitivity

imaging which contains two different types of elements arranged in an interleaved pattern (odd and even elements). The segregated elements can work individually that too at a separate frequency giving two separate transmission and reception modes. This facilitated a dual frequency probe. The low-frequency elements were set in transmission and the high-frequency elements were configured in receive mode. To accumulate the higher harmonic components collectively, a wide band pass filter was applied to the received signals. This system overcomes the limitation of bandwidth and further enhances the resolution.

This dual frequency imaging system which involves that generated harmonics will be separated by gaps in the frequency domain. The distinct troughs in the spectrum are also not found exactly in the multiples of the center frequency. This makes the separation of harmonics very difficult. That will also introduce specific artifacts visible as ripples in the echo image. So, a two-pulse technique that reduces the ripple artifacts and recovers the axial resolution was proposed [28]. It consists of transmitting two pulses with the second pulse of slightly different frequency. The sum of these two pulses in the time domain smoothen the frequency spectrum, and thus contributes to minimize these ripples. In the time domain, the sum of the two distorted pulses and the wide band filtering around the fourth harmonic is similar to critical incursion on the ripples of the superharmonic signal. This effect sharpens the superharmonic point spread function. The determination of the optimal and efficient transmission frequency in dual pulse SHI is also necessary to eliminate the real trade-off between dual pulse signal length and peak intensity. This interleaved dual pulse transducer for SHI still lacks following properties and needs considerable improvement to further enhance the SHI image quality: (i) wide bandwidth; (ii) high transmission efficiency; (iii) high sensitivity in reception and (iv) low grating lobes.

Recently, an improved interleaved phase array transducer [25] was proposed to overcome the above mentioned issues. The transducer consisted of two interleaved sub-arrays with complete 88 transducer elements (44 each for transmission and reception). The low and high frequency elements are mechanically separated and electrically decoupled. This allows to perform an optimization of parameters of each element e.g., matching layers, electrical tuning etc. The sub-array optimized for transmission had a resonance frequency of 1.0 MHz and consisted of 44 elements. The low frequency elements had a single matching layer and a backing of 3.2 MRayl. The low frequency element size was 16 × 0.2 mm and the subarray had a pitch of 0.5 mm. The subarray optimized for reception had a resonance frequency of 3.7 MHz and was composed of 44 elements. The high-frequency elements had 2 matching layers on the front and a backing with an impedance of 3.2 MRayl. The high-frequency element size was 13 × 0.2 mm, and the subarray had a pitch of 0.5 mm.

This final interleaved array transducer is facilitated with a lens for a geometrical elevated focusing of 6 cm axial distance. The total footprint of the interleaved transducer was 16 × 22 mm square. The electrical tuning of the final interleaved transducer to the imaging machine was optimized for SHI by completely analyzing the effects transmission frequency and transducer geometry. The schematic of the discussed interleaved phased array transducer designed primarily for SHI is shown in above Fig. 2.

This above discussed interleaved array transducer can also be found suitable for other imaging methods like second-harmonic, sub-harmonic, and second-order ultrasound field (SURF) [29] imaging.

Extraction of higher harmonics for SHI

In order to meet the requirement of high bandwidth, a new SHI interleaved array transducer was proposed recently. In this special array transducer, the transmit array elements operate at almost 80 % bandwidth. Initially Bouakaz et al. [10] separated superharmonic using this transducer connected to Vivid5 system (GE-Vingrncd; Horten, Norway) i.e. third, fourth and fifth harmonics using traditional band pass receiving filter in phantom based experiment. This separates harmonics by small gaps in frequency spectrum which leads to formation of ripple artifacts in superharmonic images. Furthermore, if axial receive filters are used to distinguish the received superharmonic bandwidth from the transmitted fundamental bandwidth, the axial resolution is reduced. Recently a technique named pulse inversion (PI) [30] was developed to overcome the aforementioned problem. This involves the transmission of a pulse and its inverse in parallel and further, receiving echoes of both constitutes the separation of required higher harmonics on addition. This further leads to the formation of superharmonic. However, this also introduces new disadvantage of reduction of the imaging frame rate. To overcome this, a new strategy was introduced exclusively for SHI i.e. frequency compounding either single (SPFC) or double pulse (DPFC) based on the aperture having single or interleaved transmit/receive unit, respectively.

Its implementation with real interleaved phased array transducer and the optimization of above discussed DPFC technique are proposed further by the same group [28, 31]. In this work, an interleaved array transducer of 44 elements each for transmission and reception operating at 1 MHz and 3.7 MHz, respectively. The initial prediction for the frequencies of first and second pulses as well as the pulse duration was done optimizing the performance experimentally.

DPFC surely provides the omission of multiple reflection artifacts but at the price of reduced frame rate as it constructs each trace in a post-processing stage by summing echoes from two emitted pulses, the second slightly frequency-shifted compared to the first. Danilouchkine et al. [32] has investigated the feasibility of performing the frequency compounding protocol within a single transmission, called as Single Pulse

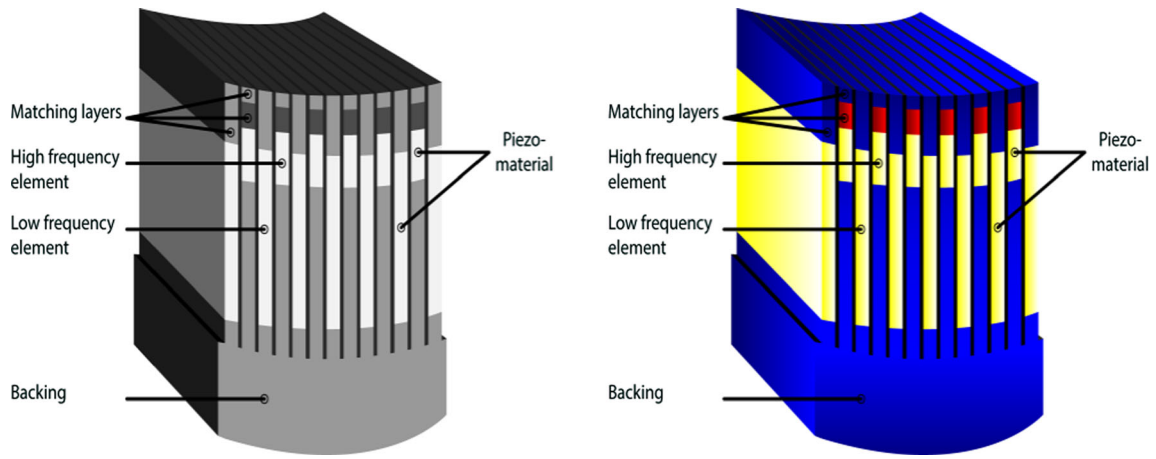

Fig. 2 The schematic of interleaved phased array transducer for SHI

Frequency Compounding (SPFC). To accomplish this, the transmit aperture is divided in two sections: first half sends pulse of lower center frequency while second half sends pulses at higher center frequency. Along with maintaining the full frame rate, it has also shown promising axial and lateral resolutions for SHI compared to the third harmonic. All the frequency compounding techniques mentioned above has been investigated theoretically and experimentally by observing the point spread function (PSF) of SHI.

Beam optimization for superharmonic imaging

The appropriate selection of imaging parameters is an essential task to achieve higher resolution imaging. The parameters like harmonic operating frequency, amplitude of acoustic pressure, aperture size, etc. shows high impact on signal to noise ratio (SNR) and penetration depth. In SHI, the frequency bandwidth like 2.5-5.5 MHz for 1 MHz operating frequency is very high compared to regular frequency bandwidths and transducer probes. This will lead to narrowing imaging bandwidth with low SNR. Similarly, the higher harmonics attenuated faster so the depth of penetration is also against the conventional.

So, Bouakaz et al. [10] carried out SHI beam optimization numerical study to decide on imaging parameters and their values for efficient imaging. The authors had investigated superharmonic generation as a function of transmitted frequency, applied acoustic pressure, grid aperture size. The study considered the conventional acoustic pressure mechanical index (MI) ranging from 0.8 to 1.8 along with transmission of three cycle Gaussian pulse of 1, 1.2 & 1.7 MHz frequency and two aperture sizes of 10 mm and 20 mm. These experimentations were carried out for SHI in comparison with fundamental and second harmonic imaging. For this, the authors not only represented the observations graphically but also shown the supremacy of SHI by calculated beam parameters like axial level, off-axis level, near field level, side lobe level, time resolution and bandwidth. The technique initially observed the variation of superharmonic amplitude at various MI at above mentioned three transmission frequencies. At higher MIs the superharmonic found better than second harmonic and with higher operating frequencies the required MI even less of the order of 1. The superharmonic energy with an optimal selection of transmitted frequency and applied acoustic amplitude exceeds the energy generated at the second harmonic frequency. In higher harmonic imaging, the attenuation generally gives hurdle of fast reduction of the energy but in this experimentation the considerable superhamonics were found available in case of 1.2 MHz transmit frequency. The other calculated beam parameters reveal the large superiority of SHI. They showed removal of near field energy by 25 dB, suppression of side lobe levels by 7.6 dB and the off axis level by 18.6 dB, improved beam width and time resolution by 20 % and 60 %, respectively. This has followed with the experimentation of observing frequency spectra for two aperture sizes at fixed MI and focal length. The amount of harmonic generation increases as aperture size reduces from 20 to 10 mm. The frequency spectrum of acoustic field at focal depth clearly shows increment of superharmonic component by 9.2 dB over 3.5 dB in second harmonic. This indicates the optimized beam formation using appropriate selection of effective instrumentation further enhances the lateral and axial resolution. Similar numerical study was carried out by Londhe and Anand [33] and Ma et al. [12] to devise the optimum beam by suitable combination of image acquisition parameters to establish the supremacy of SHI over fundamental and second harmonic. In [32], the authors had investigated the effect of variation of transmit frequency, acoustic pressure, focal depth and aperture size on SHI in comparison with fundamental and THI.

Due to frequency dependent attenuation, the amplitude of the backscattered higher harmonic echoes at the transducer surface is relatively low. So, it is an outmost importance to improve the sensitivity of the transducer to receive weak echoes successfully. In lieu of the above weakness, a second line of research of optimization of array transducer by tuning its elements i.e., their number and arrangement had been explored. Matte et al. [34] presented a new system of transducer optimization. They studied a variety of configurations between transmit and receive elements ranging from 1:1 to 1:7. Their outcomes are analyzed on basis of the ratio of harmonic peak pressure amplitudes in the main and to the side lobe. Moreover, the higher harmonic levels have been further improvised by fine tuning the transmit frequency. They observed a real trade-off between SNR and penetration depth on the basis of attenuation and nonlinearity. The special interleaved phased array transducer designed by the same group was optimized with 1:6 ratio between transmit to receive elements. This configuration has shown to have an improvement in SNR by approximately 5 dB compared to their earlier reporting with same transducer with 1:1 ratio between transmit and receive elements. It has been investigated for echocardiography and optimal transmit frequency was shown to be between 1.0 and 1.2 MHz. Similarly for abdominal imaging the optimal transmit frequency was observed between 1.7 and 1.9 MHz.

In similar second attempt, Ma et al. [15, 35], investigated transducer designs including with different transducer layouts, transmitting frequencies, and transducer materials and are compared for deciding optimized configuration to further improvise the imaging quality of contrast SHI. These comparisons are set to establish superharmonic in intravascular ultrasound (IVUS) imaging. They used stacked array transducer and proved their configuration better than the interleaved proposed by Matte et al. [34]. In transmit frequency variation, they found 7 dB improvisation on reduction of transmit frequency from 6.5 to 5 MHz at fixed received frequency of

30 MHz. In transducer material comparison, dual frequency transducer PMN-PT 1-3 composite transmitter has given higher axial resolution than single element transducer.

Nonlinear modeling of superharmonic imaging

Regarding nonlinear effects, the mathematical-physical equations that describe the propagation of acoustic waves in tissue medium are inherently nonlinear. This nonlinearity is caused by field dependent behavior of medium that is reflected in the wave equation and in the medium parameters as well [36]. In most of the phenomena and applications involving acoustic propagation, the amplitude of the acoustic waves is relatively small, and therefore a linear approximation of the nonlinear equations yields sufficiently accurate results. However, for increasing amplitude and frequency in diagnostic ultrasound for competitive high resolution of images, the nonlinear terms may not be neglected anymore and the resulting nonlinear distortion develops from weak to strong [37, 38]. For a case of plane-wave propagation in homogeneous and lossless medium, the linear propagation of an acoustic pulse with a certain amplitude and center frequency over a certain distance yields a waveform whose shape and spectrum remain the same [39]. Numerical models are essential to understand the characteristics of nonlinear wave propagation and its behavior in tissues. The numerous experimental and numerical investigations of propagation of ultrasound in different applications like breast tissue [40], abdominal wall [41], pelvic region [42], etc. are easily available in the literature. The nonlinear wave propagation is not consistent throughout the propagation distance but varies in between as it is not isolated and depends on other effects like attenuation [43] and diffraction, the source configuration, its excitation, and all effects that significantly influence the propagation of the wave need to be accounted for in a realistic and consistent way.

The development of accurate models for ultrasound propagation in soft tissue requires the consideration of three important factors: (1) Amplitude of the acoustic waves is sufficiently large causing the wave propagation to be nonlinear. For example, modern ultrasound scanners rely on nonlinear wave propagation for tissue harmonic imaging which gives images with improved clarity and contrast. (2) Properties of biological tissue (e.g., the sound speed and density) are weakly heterogeneous, with variations between the different soft tissue types and water on the order of 5 % [44]. (3) Absorption of ultrasonic frequencies with the absorption following a frequency power law. In the context of nonlinear wave propagation, an accurate model of acoustic absorption is of particular importance as the generation of higher frequency harmonics via nonlinearity is delicately balanced with their absorption.

In view of the importance of nonlinear models for the simulation of higher harmonics that may ultimately be required to validate second and higher harmonic imaging performances, we summarize here the most widely accepted numerical models.

Westervelt equation

The general wave equation that accounts for nonlinearity up to the second-order is given below the Westervelt equation [45].

$$\nabla^2 p - \frac{1}{c_0^2}\frac{\partial^2 p}{\partial t^2} + \frac{\delta}{c_0^4}\frac{\partial^3 p}{\partial t^3} = \frac{-\beta}{\rho_0 c_0^4}\frac{\partial^2 p^2}{\partial t^2}$$

where, p is the sound pressure, c_0 is the small signal sound speed, δ is the sound diffusivity, β is the non-linearity coefficient and ρ_0 is the ambient density.

The sound diffusivity δ is mathematically given as:

$$\delta = \frac{1}{\rho_0}\left(\frac{4}{3}\mu + \mu_B\right) + \frac{k}{\rho_0}\left(\frac{1}{c_v} - \frac{1}{c_p}\right)$$

where, μ is the shear viscosity, μ_B the bulk viscosity, k the thermal conductivity, c_v and c_p the specific heat at constant volume and pressure respectively.

However for wide aperture angles it is better to use the more general Westervelt equation [46, 47]. The Westervelt equation is numerically solved using a Finite Difference method [48]. The basic idea behind this method is to evaluate the PDE equation; more specifically calculate the wave amplitude, on sampling points of a computational grid. It can also be solved using Green's Function involving iterative nonlinear contrast source (INCS) approach [49, 50] and Finite Element Method [51]. It has been investigated for higher harmonics [52] using angular spectrum method and further for superhamonics by INCS approach in [13].

Burger's equation

The Westervelt equation can be simplified to take a one-dimensional form with an assumption of strictly forward propagating waves and the use of a coordinate transformation to a retarded time frame. This is known as the Burgers equation [45, 53].

$$\frac{\partial p}{\partial z} = \frac{\beta p}{\rho_0 c_0^3}\frac{\partial p}{\partial \tau} + \frac{\delta}{2c_0^2}\frac{\partial^2 p}{\partial \tau^2}$$

where, $\tau = t - z/c_0$is retarded time. The Burgers equation is the simplest model that describes the combined effects of nonlinearity and losses on the propagation of plane progressive waves. Burger's equation has been investigated in in-viscid (lossless) and viscid (lossy) domains. The viscid equation has been solved using Hopf-Cole transformation & Fay's equation

while in-viscid equation has been solved using Bessel and Fubini [54]. In-viscid is an approximation model of reality and did not account the finite size of the transducer.

Londhe and Anand [14] has investigated the superharmonic imaging for both in-viscid and viscid domains and confirmed its supremacy over fundamental and second harmonic imaging numerically. It has been further used as independent solution for solving nonlinearity in operator splitting approach based on KZK [55]. This is also solved using finite difference [56], Poisson solution [57], and spectral method [58] for observing the nonlinear propagation. This is the simplified form and useful for beginners to learn the effects of nonlinearity and absorption.

KZK equation

An augmentation to the Burgers equation that accounts for the combined effects of non-linearity, diffraction and absorption in directional sound beams is described by the Khokhlov-Zabolotskaya-Kuznetsov (KZK) equation [59, 60]. Solutions to this equation are generally used to model non-linear acoustics. If the z-axis is in the direction of the sound beam path and the (x,y) plane is perpendicular to that, the KZK equation is given as [61].

$$\frac{\partial^2 p}{\partial z \partial \tau} = \frac{c_0}{2}\nabla_\perp^2 p + \frac{\delta}{2{c_0}^3}\frac{\partial^3 p}{\partial \tau^3} + \frac{\beta}{2\rho_0 {c_0}^3}\frac{\partial^2 p}{\partial \tau^2}$$

The equation can be solved for a particular system using a finite difference scheme. Such solutions show how the sound beam distorts as it passes through a non-linear medium.

The KZK equation is valid for directional sound beams and can be applied for transducers with aperture angles smaller than 160 to 180 [62, 63]. An appropriate choice of boundary condition for the KZK equation can extend its area of applicability [64]. The multi-term Westervelt and KZK equations solved using the operator splitting approach where diffraction, attenuation and nonlinearity terms are solved individually at each step. In these, solution of nonlinearity is preferred using the solution of lossless Burger's equation [63]. The entire superharmonic imaging research groups [10, 12, 65] has used KZK equation to analyze the numerical formation of superharmonics and their propagation in tissue media.

Coded excitations for superharmonic imaging

The SHI [8] is the most talked about future of echography. The nonlinearity in sound propagation distorts the shape of wave and result in development of harmonic frequencies. Superharmonic component is comprised of all higher harmonics after second harmonic component. This can be achieved using wide band receiving filter that selects the desired higher harmonic frequencies ranging generally from third to fifth harmonic. The SNR is a key factor for ultrasound imaging; improved SNR extends the depth of penetration too. The severe frequency dependent attenuation of ultrasound signals in tissue gives weak echoes [12]. Increasing the transmitted power is again an issue as it gives heating effects. This issue can be resolved using coded excitations. The coded signals can improve the SNR without sacrificing the resolution [66, 67]. Superharmonic imaging of tissue medium with coded excitations can be recognized as "coded tissue superharmonic imaging (CSHI)" [19]. In this section, we investigate the effects of linear and nonlinear frequency modulated pulses on the performance of superharmonic imaging. So, the linear and nonlinear frequency modulated pulses are briefly described below.

Linear frequency modulated excitation (LFM pulse/chirp)

Pulse compression comprised of all the shapes with some kind of frequency modulation and its simplest form is LFM signal [67, 68]. A unit amplitude frequency modulated pulse having linear variation of instantaneous frequency f_i with time t is expressed as:

$$f_i = f_c + \frac{B}{T}t, \quad \frac{-T}{2} \le t \le \frac{T}{2}$$

where, f_c is the center frequency, B is the pulse bandwidth and T is the pulse duration. The parameter B/T is often denoted as μ, and referred to as the FM slope or the rate of FM sweep. The pulse sweeps linearly with the frequencies in the interval f_c-$B/2$ to $f_c + B/2$. The linear FM pulse with center frequency f_c is expressed as:

$$\zeta(t) = w_t(t).\exp\left[j2\pi\left(\left(f_c + \frac{B}{2}\right)t + \frac{B}{2T}t^2\right)\right]$$

Where $w_t(t)$ is a weight function. In our work, Tukey window is used as a weight function. The linear FM pulse is shown in Fig. 3 has been used in the simulations. Its frequency spectrum and time autocorrelation are also shown in Fig. 3. The LFM signal has linear change in frequency along a pulse. This could be reflected with more number of cycles but essentially maintaining short length to have better resolution.

Nonlinear frequency modulated, NLFM excitation

In one another frequency modulated signal type non-linear FM (NLFM), the frequency ramp is non-linear with steeper slope at the beginning and at the end of the pulse. The corresponding spectrum is tapered with lower magnitude at its edges [66, 67]. This spectral shaping result in the autocorrelation function exhibits attenuated side lobes. Autocorrelation function of the waveform is the output of the matched filter. Since the matched

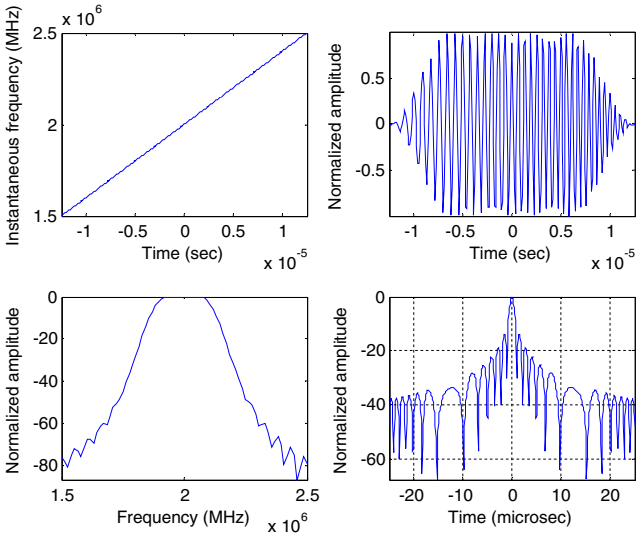

Fig. 3 **a** Instantaneous frequency vs. time, **b** LFM chirp waveform, **c** its frequency spectrum, **d** time autocorrelation function, obtained with center frequency 2 MHz, bandwidth 1 MHz and pulse duration of 25 μs

filter is used as the coding operator, the phase of the transmitted pulse will be completely canceled. Thus, the phase has no influence on the axial profile after compression.

To illustrate this, we have adapted the following derivation from [66, 67, 69] and discussed the formation of nonlinear frequency modulated pulse. The phase of the spectrum will influence the amplitude of the transmitted waveform. Most widely used polynomial phase function $\varepsilon_d(f)$, is given by [69, 70]:

$$\varepsilon_d(f) = \arg\{\mathrm{F}(\omega(n)sin(2\pi\Phi(t)))\}$$

where, $\omega(n)$ is the taper function. The phase function $\Phi(t)$ can be described as:

$$\Phi(t) = \sum_{k=0}^{S} \frac{c_k}{k!} t^k$$

where, S is the order of the polynomial, c_k are the coefficients of the polynomial. When $c_n = 0$ for $n > 2$, this reduces to the LFM chirp. We note that the instantaneous frequency $f_i(t)$ for this signal is

$$f_i(t) = \frac{d}{dt}\Phi(t) = \sum_{k=1}^{S} \frac{c_k}{(k-1)!} t^{k-1}$$

and the chirp rate is:

$$\gamma(t) = \frac{d}{dt} f_i(t) = \sum_{k=2}^{S} \frac{c_k}{(k-2)!} t^{k-2}$$

Clearly, for a phase polynomial of order N, we need a chirp rate polynomial of order $(N - 2)$. The task now becomes to find a specific $\Phi(t)$ that yields the desired $\gamma(f-f_c)$. More specifically, the task now becomes to find a specific $\gamma(t)$ that yields the desired $\gamma(f-f_c)$. $\gamma(t)$ is a function of time, whereas $\gamma_f(f)$ is the chirp rate at a particular frequency f. Initially from symmetry conditions,

$$\gamma_f(0) = \gamma(0), \quad \gamma_f\left(\frac{B}{2}\right) = \gamma\left(\frac{T}{2}\right)$$

and more generally

$$\gamma_f(f_i(t) - f_c) = \gamma(t)$$

Consequently we need to solve

$$\gamma(t) = \frac{\gamma(0)}{\omega(f_i(t) - f_c)}$$

with the constraint

$$\int_{\frac{-T}{2}}^{\frac{T}{2}} \gamma(t)dt = B$$

Here, B and T are the bandwidth and duration of pulse. This suggests the following iterative procedure for finding $\gamma(t)$

1) Select an initial $\gamma(t)$ consistent with a LFM chirp, i.e. $\gamma(t) = B/T$.
2) Integrate $\gamma(t)$ to calculate $f_i(t)$.
3) Adjust $\gamma(t)$ and $f_i(t)$ to meet the B constraint.
4) Calculate $\omega(f_i(t) - f_c)$ and then a new $\gamma(t)$.
5) Repeat steps 2–5 until convergence is achieved.

After convergence, get the instantaneous frequency function, f_i and construct the nonlinear FM signal as:

$$v(t) = sin\left(2\pi \int_0^t f_i(\tau)d\tau\right), \quad 0 \le t \le T$$

These will be basically sinusoidal pulse with nonlinearly amplitude modulation of frequency signals. It begins with lower frequencies gradually increasing, almost linear in the middle region followed by exponential sharp increase in the end. Thus making the rise of frequency along the pulse length nonlinear. Figure 4a shows the nonlinear variation of instantaneous frequency with time, the equal tapering on both sides of center frequency results by solving γ(t) according to above mentioned iterative procedure. Figure 4b shows the 2 MHz, 1 MHz bandwidth nonlinear FM pulse generated and Fig. 4c shows its time autocorrelation function. It is expected that any practical range sidelobe filtering can be accomplished more efficiently by selecting a corresponding NLFM waveform compared to generally used window functions. Matched filter output results will be identical excluding an increase in SNR using the NLFM waveform.

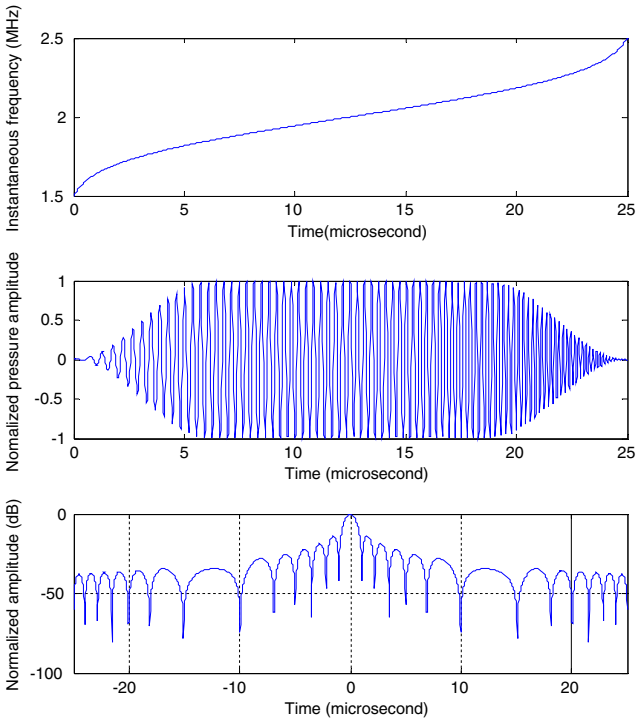

Fig. 4 **a** Instantaneous frequency variation with pulse time, **b** normalized NLFM pulse and **c** the autocorrelation function obtained with center frequency, $fc = 2$ MHz, bandwidth, $\Delta f = 1$ MHz (0.5) and pulse duration of 25 μs

Coded superharmonic imaging

In order to study the effects of linear and nonlinear frequency modulated excitations on superharmonic imaging, two mathematical solutions of nonlinear wave equation have been used to generate the superharmonic field and also fundamental and second harmonic for comparison. The angular spectrum method [58] based combined time and frequency domain solution which consisted of solution of consecutive attenuation and diffraction in time domain followed by nonlinearity term in frequency domain at each successive step of propagation. This numerical study is based on following input excitation and medium parameters. The numerical results in this section are reproduced from [19].

Using LFM/Chirp The LFM pulse derived in above section is applied here. Figure 5a shows the linear FM modulated pulse applied for stimulating a circular ultrasound transducer for imaging. The medium and transducer parameters mentioned in Table 2 have been used in this part of the wok. The axial spectral profiles of fundamental, second harmonic and superharmonic are shown in Fig. 5b. The second harmonic energy is laying 50 dB below fundamental energy while superharmonic energy is 43 dB below fundamental at the surface of the transducer. The superharmonic field constructs very faster along propagation distance and also becomes maximum at focal point. After focusing point, it remains close to second harmonic and by the end of propagation distance

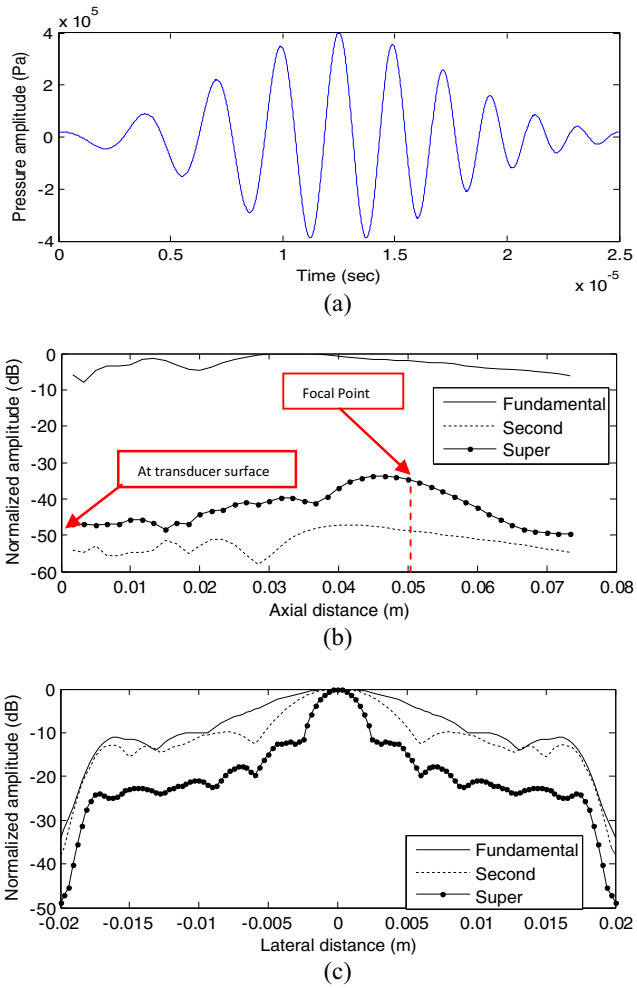

Fig. 5 **a** Linear FM (chirp) signal of centre frequency, $f_c = 2.0$ MHz and bandwidth, BW = 0.5. **b** Axial spectral profiles and **c** lateral spectral profiles at z = 50 mm of fundamental (*solid*), second harmonic (*dashed*) and superharmonic (*dotted*) frequency components. (Reproduced from [19])

superharmonic remains 43 dB below fundamental while second harmonic 48 dB below fundamental energy. So superharmonic imaging with linear FM modulated excitation energy shows potential at imaging distances. Figure 5c shows the lateral spectral profiles of fundamental, second harmonic and superharmonic frequency components. From Fig. 5c, the beam width of superharmonic at 10 dB has been found to be 3.95 mm and for second and fundamental, 9.48 mm and 19.27, respectively. This clearly point to better lateral resolution for superharmonic imaging is over second harmonic and fundamental imaging, using linear FM excitation. Moreover, the sufficient gathering of superharmonic energy in the central part of the beam has been observed along with adequate reduction in side lobes.

The superharmonic energy available for scattering is 12.54 dB below fundamental energy while second harmonic energy has higher scattering energy available at 10.14 dB below fundamental energy. So the scattering from the objects

Table 2 Parameters used in following numerical experimentation

Parameter		Values
Medium parameters		
Nonlinear coefficient	B/A	5
Peak pressure	P_0	400 kPa
Density	ρ	1000 kg/m^2
Speed of sound	c	1540 m/s
Attenuation coefficient	α	0.5
Power law	b	1
Transducer parameters		
Transducer type		'Circular'
Transducer radius	a	0.015 m
Azimuthal focal length	Fa	0.05 m
Elevation focal length	Fe	0.05 m

located at the edges of the beam will be less in superharmonic as compared to second harmonic imaging.

To better present the outcomes, the Fig. 6 represents the elevation views of simulated three imaging fields. Figure 6a shows the complete field distribution in elevation view while Fig. 6b–d show the fundamental, second harmonic and superharmonic field distributions of the transducer over a plane defined by the axial and lateral coordinate axes. The ultrasound field of the fundamental beam is distributed in number of side lobes and the beam width is more. This confirms the side lobe artifacts in the fundamental image. The side lobes in the second harmonic are more in number as compared to fundamental but the beam width is 50 % lower than the fundamental. This assures the improved SNR but numerous clutters due to sidelobes. In case of superharmonic beam, the minimum side lobes of lower amplitude are present and the beam is further narrowed to 25 % that of fundamental. This indicates the minimum clutter artifacts and high resolution in case of superharmonic imaging.

Using NLFM Chirp The frequency ramp derived from earlier equation given in section B, visually shown in Fig. 7a, is nonlinear, steeper slope at start and end and almost linearly increasing in between of the pulse. The corresponding pulse (Fig. 7b) is tapered with lower magnitude at its edges. This spectral shaping result in the autocorrelation function exhibiting attenuated side lobes, limited to less than −35 dB in Fig. 7c. It can also be observed that the second harmonic energy is 82 dB below fundamental energy while superharmonic energy is almost less than 100 dB below fundamental at the surface of the transducer. At the entry of the body, superharmonics is almost absent as actual, indicates the substantial reduction of reverberations in SHI. Superharmonics gradually build thereafter reaching to maximum near focal point.

From Fig. 7d, the beam width of superharmonic has been found to be 1.45 mm while it is 2.96 mm and 3.6 mm for second harmonic and fundamental components, respectively. Thus, the beam further narrows with nonlinear FM chirp as compared to linear FM chirp. With nonlinear FM excitation, the lateral resolution is improved further. At the same time, the side lobe suppression is also higher with nonlinear FM excitation. But the acoustic energy of the superharmonic is 120 dB below fundamental, so the poor reflections may cause problem in image formation. From Fig. 7d, it is evident that the

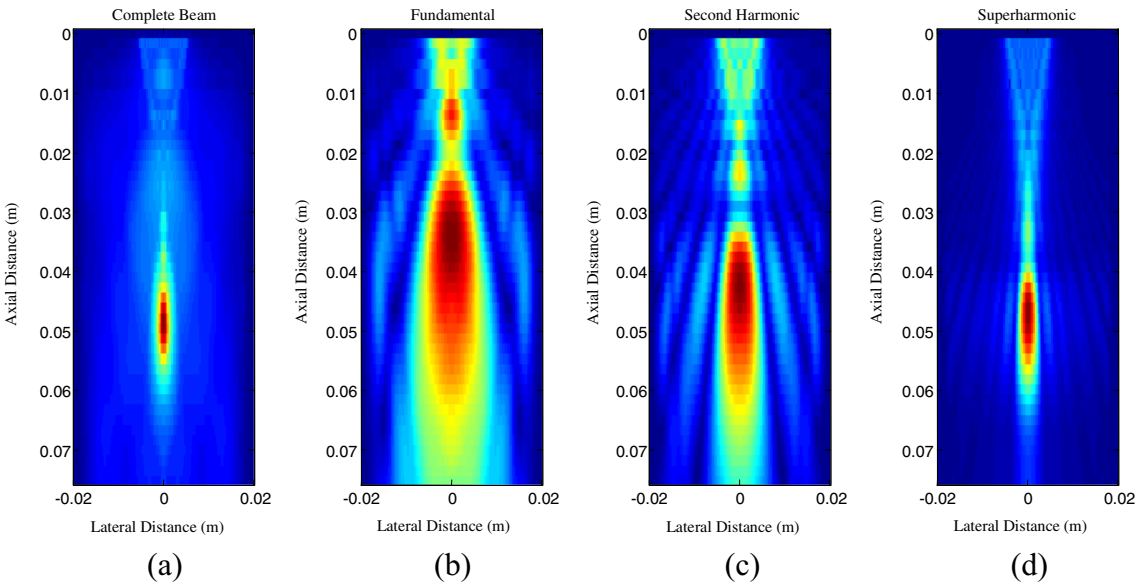

Fig. 6 Azimuthal spectral profiles for a 2 MHz circular transducer of radius 10 mm and focusing of 50 mm in both azimuthal and elevation directions. **a** Complete beam spectral profile, **b** fundamental spectral profile, **c** second harmonic spectral profile and **d** superharmonic spectral profile. (Reproduced from [19])

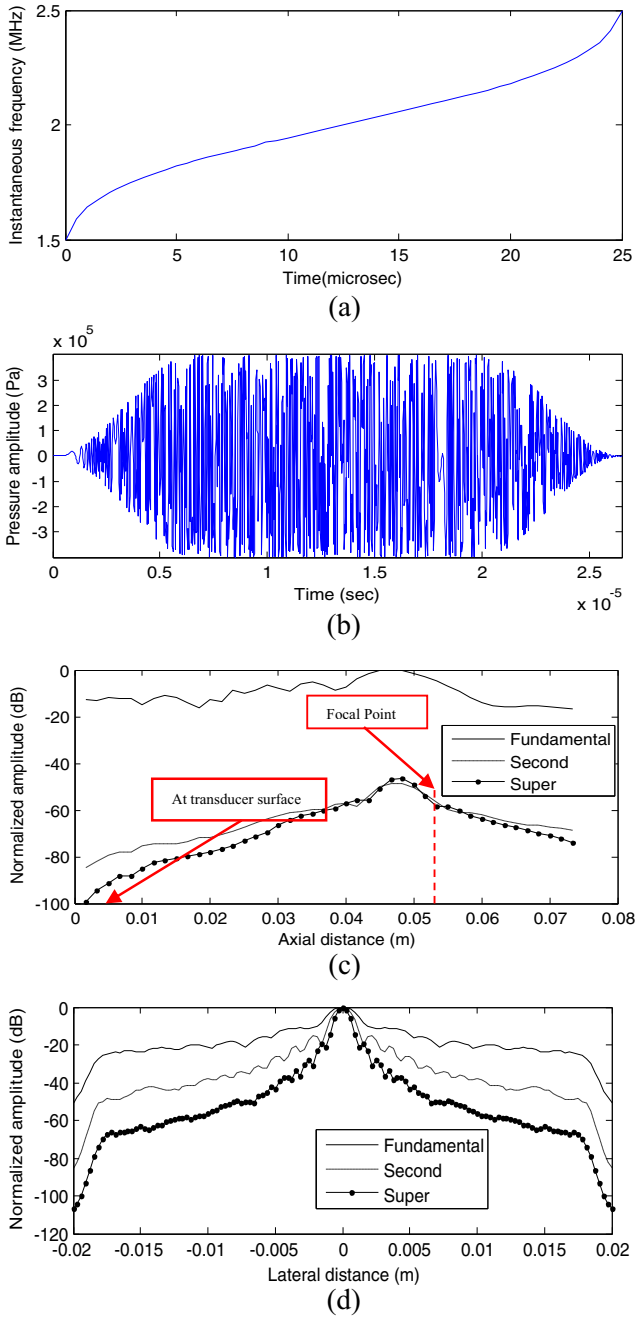

Fig. 7 **a** Instantaneous frequency pattern given by the polynomial in equation (6.9), **b** nonlinear FM signal of centre frequency, fc = 2.0 MHz and bandwidth, BW = 0.5. **b** Axial spectral profiles and **c** lateral spectral profiles at z = 35 mm of fundamental (*solid*), second harmonic (*dashed*) and superharmonic (*dotted*) frequency components. (Reproduced from [19])

scattering energy level is declined further in superharmonic imaging with nonlinear FM chirp (−36.02 dB) compared to linear chirp (−12.54). Similarly, the significant side lobe level improvement from −10.14 to −20.03 dB can be seen in second harmonic component too. Using this method, the presence of second or superharmonic near surface of the transducer is found very less. The supeharmonic and second harmonic builds up and becomes maximum at focal depth.

Figure 8a shows the complete field distribution while Fig. 8b–d show the fundamental, second harmonic and superharmonic field distributions of the transducer over a plane defined by the axial and lateral coordinate axes. The superharmonic beam is the narrowest as compared to the beams generated with earlier excitation techniques. The second harmonic field is also improved with almost negligible sidelobes and smaller beamwidth. This confirms the better image formation using nonlinear FM chirps in second and superharmonic imaging.

The main results from the study are summarized in Table 3 for all three excitation techniques. The first column shows axial levels at the focus, second column shows the beam widths of −10 dB at the mid propagation distance while last column indicates the side lobe suppression parameter PSL for fundamental, second harmonic and superharmonic components.

The SHI and THI takes the benefit of the nonlinear wave propagation of ultrasound waves in tissue and the associated generation of higher harmonics to obtain improved resolution images. However, the higher harmonics are weak initially and further weaken due to frequency dependent attenuation as compared to fundamental frequency component; it may be beneficial to use coded excitations to improve SNR and penetration depth. There are significant observations indicated in the results in above section pertaining to propagation of conventional, linear FM and nonlinear FM pulses, such improvement in resolution, SNR and penetration depth in case of second harmonic and superharmonic components.

Superharmonic frequency component of the distorted ultrasound wave provides considerable enhancement in resolution. This has been reported earlier by various researchers. But with the coded excitation, the resolution has been further improved. The beam width of superharmonic lateral beam profile is reduced minutely with linear FM pulse (Fig. 5c) as compared to conventional short pulse, but with nonlinear FM excitation (Fig. 7d), the beam width has reduced substantially which is almost three times. On the same line, the second harmonic imaging has also shown significant improvement in lateral resolution with nonlinear FM excitation. For conventional second harmonic imaging, lower and narrower bandwidths used to be selected for both transmission and reception to avoid overlapping of fundamental and second harmonic but with the use of wide band receive filter for superharmonic imaging will ultimately lead to improved axial resolution.

The superharmonic component with all three types of excitation enters in the body with lower energy levels. This may avoid the image artifacts because of reverberations at the boundaries of the body. The linear summation of higher harmonics enhances the energy levels of superharmonic component as compared to second harmonic and accordingly improves the SNR with conventional and linear FM (Figs. 5b and 7b) excitations. While with nonlinear FM excitation,

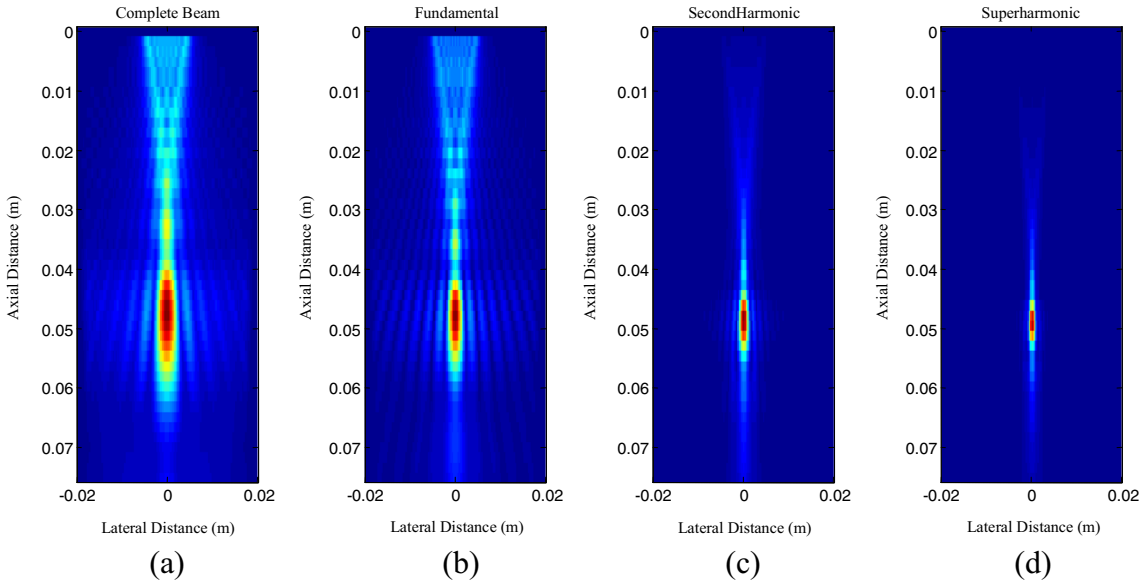

Fig. 8 Azimuthal spectral profiles for a 2 MHz circular transducer of radius 10 mm and focusing of 50 mm in both azimuthal and elevation directions. **a** Complete beam spectral profile, **b** fundamental spectral profile, **c** second harmonic spectral profile and **d** superharmonic spectral profile. (Reproduced from [19])

pt?>superharmonic level at focal point is higher which leads to the considerable improvement in SNR. In nonlinear CTHI, medium nonlinearity must be causing generation of multiple frequencies like harmonics and their intermodulations. This may lead to strong superharmonic field which will accordingly improve the SNR. After the focal point, the superharmonic starts to attenuate with higher rate in case of conventional and linear FM while it attenuates with very slower rate in nonlinear FM imaging. The peak side lobe level encounters substantial improvement with nonlinear FM excitation (−36.02 dB) as compared to conventional short pulse (−12.45 dB) and linear FM excitation (−12.54 dB). The nonlinear frequency distribution across the duration of pulse leads to significant suppression of side lobes. So, the scatterers come in the region of beam edges which reduces the noise level in ultrasound images and maximum acoustic energy can be focused on testing object. This leads to improved SNR (by almost 24 dB) and penetration depth as well. It has also been found that there is also a considerable enhancement of SNR (almost 10 dB) in nonlinear CTHI as compared to THI and linear CTHI.

Comparative overview of present results with literature

There are two important references [10, 12] in the literature who have evaluated the supeharmonic imaging numerically as well as experimentally and confirmed the advantage of superharmonic imaging over fundamental and second harmonic imaging. The numerical analysis of supeharmonic imaging reported in [10] has been summarized in Table 4.

The simulation done in paper [10] is based on plane circular transducer of 20 mm diameter and center frequency of 1.7 MHz and MI (mechanical index) of 1.3 (i.e. peak pressure amplitude of 1.7 MPa). The focus was set to 60 mm. The other relevant medium parameters considered are attenuation coefficient $\alpha = 0.5$ dB/cm at 1 MHz with frequency dependence of f1and coefficient of nonlinearity β was set to 4.75.

Even though the initial parameters adapted for studies done in here are different, it can be easily understand that the superharmonic imaging using coded excitations follows the claims made in [10]. The performance came with combined time and frequency domain with conventional Gaussian pulse

Table 3 Comparison of Beam Parameters at Fundamental, Second Harmonic and Superharmonic Components with Three Excitation Schemes

	Short Gaussian pulse			LFM pulse			NLFM pulse		
	Axial Level (dB)	Peak side-lobe level, PSL (dB)	Beam-width (mm)	Axial Level (dB)	Peak side-lobe level, PSL (dB)	Beam-width (mm)	Axial Level (dB)	Peak side-lobe level, PSL (dB)	Beam-width (mm)
Fundamental	−1.12	−11.26	7.32	−2.08	−10.31	13.27	−1.03	−11.65	3.60
Second harmonic	−32.09	−10.11	8.54	−52.11	−10.14	9.48	−49.06	−20.03	2.96
Superharmonic	−12.10	−12.45	4.65	−34.05	−12.54	3.95	−48.0	−36.02	1.45

Table 4 Numerical Results from Bouakaz et al. [10]

Bouakaz et al. [10]		Axial level (dB)	Peak Side lobe level PSL (dB)	Beam width (mm)
Conventional Gaussian pulse (Time domain solution of KZK equation)	Fundamental	0	0	5.3
	Second harmonic	−6.9	−4.6	3.5
	Superharmonic	−3	−11.6	2.6

is quite deviating from the performance reported in Table 4 with time domain solution of KZK equation. This must be due to the different initial parameters and observation conditions. In Table 4, the axial level (−3.0 dB) at focal depth achieved by the superharmonic field is very less as compared as compared to the axial levels achieved for superharmonic field by linear FM pulse (−34 dB) and nonlinear FM pulse (−48 dB). The even better axial levels are achieved in the second harmonic imaging. This suggests that the by using linear FM and nonlinear FM pulses, the effect of higher harmonics are less near the surface of the transducer. This is very important for reducing the effects of aberration and reverberation which causes harmonic leakage at the boundary of transducer and body wall. The best axial level comes from the use of nonlinear FM pulse as excitation.

In Table 4, the PSL given is just −11.6 dB for superharmonic; the similar PSLs are achieved with conventional and linear FM pulse. But with nonlinear FM pulse, the three times higher PSL can be achieved as compare to the PSL from Table 3. The greater suppression of side-lobes confirms the low clutter artifacts in the images that enhances lateral as well as contrast resolution. The beam width of the linear FM pulse is very poor but with the nonlinear FM pulse the lowest beam width of 1.45 mm among all has been achieved for superharmonic imaging. The beam width of superharmonic field is almost 50 % reduced with nonlinear FM pulse as compared to the beamwidth reported in [10]. So it is needed to be believed that with coded excitation, the further improvement in the quality image parameters is very assured. Even the second harmonic is also seeing quite improved with coded excitation. The computational methods adapted in Tables 3 and 4 differs in the results of conventional pulse excitation but indicates the similar success for superharmonic imaging over fundamental and second harmonic imaging.

Future of SHI

SHI is still in infancy stage and needs to be grown ahead. The truth of enhanced resolution with increase in frequency cannot be neglected. Though, the penetration depth reduces with frequency, it is found acceptable in SHI which has been experimentally found good in Echocardiography. There is a clear scope of improvement in SHI when it comes to penetration depth. This will help in imaging complex body organs which are distantly deep. SHI can be improved further when it comes to optimization of beam-forming, hardware, novel excitations and reception.

The numerical studies show further improvement with coded excitations in SHI which has not been validated yet with real in-vivo or in-vitro experimentations. This needs further attention as we can observe rising improvement in SONAR with coded excitations. The tradeoff between coding methods, resolution and penetration depth has to be observed critically organ wise. It may need to set separate SHI image standards for various organs in the body. The linear and nonlinear coded excitations can have plenty of variants alone with changing sweep.

The specialized array transducer designed by A. Bouakaz and team only follow the aspect of resolution improvement. Further hardware arrangement of reducing attenuation or growing pulse amplitude can be made. The hardware following FDA ultrasound MI (mechanical index) limitation and SHI field propagation needs serious check and respective research. The formation of harmonics due to nonlinear propagation and reaching to their zenith is around the focal depth. These harmonics attenuate while travelling back for image formation. The synthetic harmonics may be generated by transducer and SHI formation may be observed on specific harmonics selection. This could be better handle using the optimization of beam. The beam optimization for highest and quality outcome has been in studied in recently [34, 71–74]. The same can be tried on complex multi harmonic SHI beam. There are plenty of optimization algorithms adaptive; variance based [34, 71–74] which may help selecting best combination of hardware and soft parameters.

Conclusion

In fundamental imaging, the field attenuates with depth of penetration. The same prevents the harmonics to use for imaging but attenuation is counter balanced by field generated by cumulative addition of harmonics. The challenge of high resolution is slowly being attended by SHI with design of transducer and harmonics extraction method. The interleaved array transducer for SHI is sensitive to harmonics and its structure promotes the Single Pulse Frequency Compounding which extracts the harmonics with reduced artifacts and frame rate. The further implementation of SHI using coded excitations has taken it to new heights where its efficient interaction with tissues increases not only strength of

harmonics but also promises towards improved resolution. The shorter coded pulses and narrow beam encourages further improvement in the axial and lateral resolution, respectively. SHI is being found successful in echocardiography, angiography, IVUS, abdominal ultrasound in reported experiments in the literature. It could also be useful blood vessel wall, anterior segments of the eye and skin or small animal scanning. This can solely serve the purpose of ultrasound scanning of various organs in moderate to high frequency imaging.

The beam optimization, coded excitation in SHI has great scope and may further enhance it. This paper is state-of-art and demonstrated same with reporting experimentations and its interpretation from the literature.

References

1. Whittingham, T., Tissue harmonic imaging. *Eur. Radiol.* 9(3): S323–S326, 1999.
2. Ward, B., Baker, A. C., and Humphrey, V. F., Nonlinear propagation applied to the improvement of resolution in diagnostic medical ultrasound. *J. Acoust. Soc. Am.* 101(1):143–154, 1997.
3. Starritt, H. C., Duck, F. A., Hawkins, A. J., and Humphrey, V. F., The development of harmonic distortion in pulsed finite-amplitude ultrasound passing through liver. *Phys. Med. Biol.* 31(12):1401–1409, 1986.
4. Starritt, H., Perkins, M., Duck, F., and Humphrey, V., Evidence for ultrasonic finite-amplitude distortion in muscle using medical equipment. *J. Acoust. Soc. Am.* 77(1):302–306, 1985.
5. Muir, T. G., Nonlinear effects in acoustic imaging. *Acoust. Imaging* 9:93–109, 1980.
6. Duck, F. A., Nonlinear acoustics in diagnostic ultrasound. *Ultrasound Med. Biol.* 28(1):1–18, 2002.
7. Averkiou, M., Tissue harmonic imaging. *Ultrasonics Symposium, 2000 IEEE*, 2, 1563-1572, 2000.
8. Shen, C., and Li, P., Harmonic leakage and image quality degradation in tissue harmonic imaging. *IEEE Trans. Ultrason. Ferroelectr. Freq. Control* 48(3):728–736, 2001.
9. Bouakaz, A., Frigstad, S., ten Cate, F. J., and de Jong, N., Super harmonic imaging: A new imaging technique for improved contrast detection. *Ultrasound Med. Biol.* 28(1):59–68, 2002.
10. Bouakaz, A., and de Jong, N., Native tissue imaging at superharmonic frequencies. *IEEE Trans. Ultrason. Ferroelectr. Freq. Control* 50(5):496–506, 2003.
11. Bouakaz, A., Krenning, B. J., Vletter, W. B., ten Cate, F. J., and Jong, N. D., Contrast superharmonic imaging: A feasibility study. *Ultrasound Med. Biol.* 29(4):547–553, 2003.
12. Ma, Q., Zhang, D., Gong, X., and Ma, Y., Investigation of superharmonic sound propagation and imaging in biological tissues in vitro. *J. Acoust. Soc. Am.* 119(4):2518–2523, 2006.
13. van Neer, P. L. M. J., Danilouchkine, M. G., Verweij, M. D., Demi, L., Voormolen, M. M., van der Steen, A. F. W., and de Jong, N., Comparison of fundamental, second harmonic, and superharmonic imaging: A simulation study. *J. Acoust. Soc. Am.* 130(5):3148–3157, 2011.
14. Londhe, N. D., and Anand, R. S., Investigation of ultrasonic shock wave propagation and superharmonic field generation in human soft tissues. *Int. J. Math. Model. Numer. Optimisation* 1(4):316–329, 2010.
15. Ma, J., Martin, K. H., Li, Y., Dayton, P. A., Shung, K. K., Zhou, Q., and Jiang, X., Design factors of intravascular dual frequency transducers for super-harmonic contrast imaging and acoustic angiography. *Phys. Med. Biol.* 60(9):3441–3457, 2015.
16. Bouakaz, A., Ten Cate, F. J., and de Jong, N., A new ultrasonic transducer for improved contrast nonlinear imaging. *Phys. Med. Biol.* 49(16):3515–3525, 2004.
17. Ma, J., Jiang, X., Martin, K. H., Dayton, P. A., Li, Y., Zhou, Q., Dual frequency transducers for intravascular ultrasound superharmonic imaging and acoustic angiography. *Ultrasonics Symposium (IUS), 2014 I.E. International*, 675-678 (3-6 Sept. 2014).
18. Danilouchkine, M. G., van Neer, P. L. M. J., Matte, G. M., Voormolen, M. M., Verweij, M. D. and de Jong, N., Superharmonic imaging based on chirps. *IEEE Ultrasonics Symp.* 2195-2198, 2010.
19. Londhe, N. D., and Anand, R. S., Coded Tissue Superharmonic Imaging: An analytical study. *J. Med. Ultrasound* 20(2):101–108, 2012.
20. Londhe, N. D., and Anand, R. S., Numerical Investigation of Superharmonic Imaging Using Chirp Excitation. *J. Med. Ultrasound* 19(3):81–86, 2011.
21. Hossack, J. A., Mauchamp, P., and Ratsimandresey, L., A high bandwidth transducer optimized for harmonic imaging. In: *Proc. IEEE Ultrason. Symp.* 2, 1021–1024, 2000.
22. Akiyama, I., Saito, S., and Ohya, A., Development of an ultra-broadband ultrasonic imaging system: Prototype mechanical sector device. *J. Med. Ultrasound* 33(2):71–76, 2006.
23. Ferin, G., Legros, M., Felix, N., Notard, C., and Ratsimandresey, L., 3F-6 Ultra-wide bandwidth array for new imaging modalities. In: *Proc. IEEE Ultrasonic Symp.* New York, NY, 204–207, 2007.
24. Zhou, S., Reynolds, P., and Hossack, J. A., Improving the performance of capacitive micromachined ultrasound transducers using modified membrane and support structures. In: *Proc. IEEE Ultrasonic Symp.* Rotterdam, The Netherlands, 4,1925–1928, 2005.
25. van Neer, P. L. M. J., Matte, G., Danilouchkine, M. G., Prins, C., van den Adel, F., and de Jong, N., Super-harmonic imaging: development of an interleaved phased-array transducer. *IEEE Trans. Ultrason. Ferroelectr. Freq. Control* 57(2):455–468, 2010.
26. Forsberg, F., Shi, W., Jadidian, B., and Winder, A., Design and acoustic characterization of a multi-frequency harmonic array for nonlinear contrast imaging. *Ultrasonics Symposium, 2001 IEEE*, 2, 1721-1724, 2001
27. Forsberg, F., Shi, W., Jadidian, B., and Winder, A., Multi-frequency harmonic arrays: Initial experience with a novel transducer concept for nonlinear contrast imaging. *Ultrasonics* 43(2):79–85, 2004.
28. van Neer, P. L. M. J., Danilouchkine, M. G., Matte, G. M., van der Steen, A. F. W., and de Jong, N., Dual-pulse frequency compounded superharmonic imaging. *IEEE Trans. Ultrason. Ferroelectr. Freq. Control* 58(11):2316–2324, 2011.
29. Masoy, S. E., Standal, O., Nasholm, P., and Johansen, T. F., SURF imaging: In vivo demonstration of an ultrasound contrast agent detection technique. *IEEE Trans. Ultrason. Ferroelectr. Freq. Control* 55(5):1112–1121, 2008.
30. Ma, Q., Ma, Y., Gong, X., and Zhang, D., Improvement of tissue harmonic imaging using the pulse-inversion technique. *Ultrasound Med. Biol.* 31(7):889–894, 2005.
31. Verweij, M. D., Demi, L., van Neer, P. L. M. J., Danilouchkine, M. G., de Jong, N., and van Dongen, K. W. A., A dual pulse technique for improving the point spread function of superharmonic imaging systems. *J. Acoust. Soc. Am.* 129(4):2611, 2011.
32. Danilouchkine, M. G., van Neer, P. L. M. J., Verweij, M. D., Matte, G. M., Vletter, W. B., van der Steen, A. F. W., and de Jong, N., Single pulse frequency compounding protocol for superharmonic imaging. *Phys. Med. Biol.* 58(14):4791–4805, 2013.
33. Londhe, N. D., and Anand, R. S., Numerical investigation of non–linear propagation of amplitude–modulated ultrasound pulses in

human soft tissues and superharmonic beam optimization. *Int. J. Biomed. Eng. Technol.* 8(1):82–98, 2012.
34. Matte, G., Van Neer, P., Danilouchkine, M., Huijssen, J., Verweij, M., and De Jong, N., Optimization of a phased-array transducer for multiple harmonic imaging in medical applications: frequency and topology. *IEEE Trans. Ultrason. Ferroelectr. Freq. Control* 58(3): 533–546, 2011.
35. Ma, J., Martin, K. H., Dayton, P. A., and Xiaoning, J., A preliminary engineering design of intravascular dual-frequency transducers for contrast-enhanced acoustic angiography and molecular imaging. *IEEE Trans. Ultrason. Ferroelectr. Freq. Control* 61(5):870–880, 2014.
36. Muir, T. G., and Carstensen, E. L., Prediction of nonlinear acoustic effects at biomedical frequencies and intensities. *Ultrasound Med. Biol.* 6(4):345–357, 1980.
37. Baker, A. C., Nonlinear pressure fields due to focused circular apertures. *J. Acoust. Soc. Am.* 91(2):713–717, 1992.
38. Baker, A. C., Berg, A. M., and Tjotta, J. N., The nonlinear pressure field of plane, rectangular apertures: Experimental and theoretical results. *J. Acoust. Soc. Am.* 97(6):3510–3517, 1997.
39. Baker, A. C., and Humphrey, V. F., Distortion and high frequency generation due to nonlinear propagation of short pulses from a plane circular piston. *J. Acoust. Soc. Am.* 92(3):1699–1705, 1992.
40. Douglas Mast, T., Two- and three-dimensional simulations of ultrasonic propagation through human breast tissue. *Acoust. Res. Lett. Online* 3(2):53–58, 2002.
41. Douglas Mast, T., Hinkelman, L. M., Orr, M. J., Sparrow, V. W., and Waag, R. C., Simulation of ultrasonic pulse propagation through the abdominal wall. *J. Acoust. Soc. Am.* 102(2):1177–1190, 1997.
42. Desser, T. S., Jeffrey, R. B., Lane, M. J., and Ralls, P. W., Pictorial essay: Tissue harmonic imaging: Utility in abdominal and pelvic sonography. *J. Clin. Ultrasound* 27(3):135–142, 1999.
43. Wallace, K. D., Holland, M. R., and Mille, J. G., Improved description of shock wave evolution in media with frequency power law dependent attenuation. *J. Acoust. Soc. Am.* 109(5):2263–2265, 2001.
44. Szabo, T. L., *Diagnostic Ultrasound Imaging*. Elsevier, Burlington, 2004.
45. Hamilton, M. F., and Blackstock, D. T., *Nonlinear acoustics*. Academic, San Diego, 1998.
46. Tavakkoli, J., Cathignol, D., Souchon, R., and Sapozhnikov, O. A., Modeling of pulsed finite-amplitude focused sound beams in time domain. *J. Acoust. Soc. Am.* 104(4):2061–2072, 1998.
47. Yuldashev, P. V., and Khokhlova, V. A., Simulation of three-dimensional nonlinear fields of ultrasound therapeutic arrays. *Acoust. Phys.* 57(3):334–343, 2011.
48. Cohen, G., and Joly, P., Construction and Analysis of Fourth-Order Finite Difference Schemes for the Acoustic Wave Equation in Nonhomogeneous Media. *SIAM J. Numer. Anal.* 33(4):1266–1302, 1996.
49. Huijssen, J., and Verweij, M. D., An Iterative Method for the Computation of Nonlinear Wide-Angle Pulsed Acoustic Fields of Medical Diagnostic Transducers. *J. Acoust. Soc. Am.* 127(1):33–44, 2010.
50. Libertario, D., Verweij, M. D., and van Dongen, K. W. A., Modeling three-dimensional nonlinear acoustic wave fields in media with spatially varying coefficient of nonlinearity, attenuation and speed of sound. *Ultrasonics Symposium (IUS), 2012 I.E. International*. 519-522, 2012
51. Dirkse, B., finite element method applied to the one-dimensional westervelt equation. 2014.
52. Pasovic, M., Donilouchkine, M., van der Steen, A., Basset, O., de Jong, N., and Cachard, C. Extended angular spectrum method for calculation of higher harmonics. *10ème CongrèsFrançaisd'Acoustique.* 2010.
53. Burgers, J. M., A mathematical model illustrating the theory of turbulence. *Adv. Appl. Mech.* 1:171–199, 1948.
54. Blackstock, D. T., Connection between the Fay and Fubini solutions for plane sound waves of finite amplitudes. *J. Acoust. Soc. Am.* 39(6):1019–1026, 1966.
55. Lee, Y. S., and Hamilton, M. F., Time-domain modeling of pulsed finite amplitude sound beams. *J. Acoust. Soc. Am.* 97(2):906–917, 1995.
56. Schiffner, M., Mleczko, M., Schmitz, G., Evaluation of an analytical solution to the Burgers equation based on Volterra series. *Ultrasonics Symposium (IUS), 2009 I.E. International*, 1-4(20-23 Sept. 2009).
57. Jensen, J. A., Fox, P. D., Wilhjelm, J., and Taylor, L. K., Simulation of non-linear ultrasound fields. *In Proc. IEEE Ultrason. Symp.*, 2, 1733–1736, 2002.
58. Zemp, R. J., Tavakkoli, J., and Cobbold, R. S. C., Modeling of nonlinear ultrasound propagation in tissue from array transducers. *J. Acoust. Soc. Am.* 113(1):139–152, 2003.
59. Rozanova-Pierrat, A., Mathematical analysis of Khokhlov-Zabolotskaya-Kuznetsov (KZK) equation. 2006.
60. Kuznetsov, V. P., Equations of nonlinear Acoustics. *Sov. Phys. Acoust.* 16(4):467–470, 1971.
61. Humphrey, V. F., Non- propagation for linear medical imaging. *WCU* 2003:73–80, 2003.
62. Tjotta, J. N., Tjotta, S., and Vefring, E. H., Effects of focusing on the nonlinear interaction between two collinear finite amplitude sound beams. *J. Acoust. Soc. Am.* 89(3):1017–1027, 1991.
63. Soneson, J. E., A parametric study of error in the parabolic approximation of focused axisymmetric ultrasound beams. *J. Acoust. Soc. Am.* 131(6):EL481–EL485, 2012.
64. Canney, M. S., Bailey, M. R., Crum, L. A., Khokhlova, V. A., and Sapozhnikov, O. A., Acoustic characterization of high intensity focused ultrasound fields: A combined measurement and modeling approach. *J. Acoust. Soc. Am.* 124(4):2406–2420, 2008.
65. Londhe, N. D., and Anand, R. S., Numerical Parametric Study of Superharmonic Field Properties in Nonlinear Ultrasound Wave Propagation in Human Soft Tissues. *Acta Acustica United Acustica* 98(1):179–187, 2012.
66. Misaridis, T., and Jensen, J. A., Use of modulated excitation signals in medical ultrasound. Part I: Basic concepts and expected benefits. *IEEE Trans. Ultrason. Ferroelectr. Freq. Control* 52(2):177–191, 2005.
67. Misaridis, T., and Jensen, J. A., Use of modulated excitation signals in medical ultrasound. Part II: Design and performance for medical imaging applications. *IEEE Trans. Ultrason. Ferroelectr. Freq. Control* 52(2):192–207, 2005.
68. Song, J., Kim, S., Sohn, H., Song, T., and Yoo, Y. M., Coded excitation for ultrasound tissue harmonic imaging. *Ultrasonics* 50(6):613–619, 2010.
69. Misaridis, T., Ultrasound imaging using coded excitations. PhD Thesis, The Technical University of Denmark, 2001.
70. Doerry, A. W., Generating nonlinear FM chirp waveforms for radar. *Sandia Report SAND2006-5856*, Unlimited Release, 2006.
71. Xia, X.-y. et al., Robust minimun variance beamforming applied to ultrasound imaging in the presence of phase aberration. *Piezoelectricity, Acoustic Waves, and Device Applications (SPAWDA), Symposium on*. IEEE, 2014.
72. Avanji, S. A. I., Far, A. M., Asl, B. M., Investigation of the effects of transducer Parameters on adaptive MV beamformers in medical ultrasound applications. In: *Electrical Engineering (ICEE), 21st Iranian Conference,* pp. 1-6, 2013
73. Chen, J., Yiu, B., So, H. K. H., & Yu, A. C., Real-time GPU-based adaptive beamformer for high quality ultrasound imaging. In: *Ultrasonics Symposium (IUS), IEEE International* (pp. 474-477), 2011.
74. Qin, Y., Wang, Z., Ingram, P., Li, Q., and Witte, R. S., Optimizing frequency and pulse shape for ultrasound current source density imaging. *IEEE Trans. Ultrason. Ferroelectr. Freq. Control* 59(10):2149–2155, 2012.